Materials Chemistry and Physics 124 (2010) 713–719

Contents lists available at ScienceDirect

Materials Chemistry and Physics

journal homepage: www.elsevier.com/locate/matchemphys

Synthesis, characterization and catalytic evaluation of cubic ordered mesoporous iron–silicon oxides

T.S. Martins[a,*], A. Mahmoud[c], L.C. Cides da Silva[c], I.C. Cosentino[e], M.H. Tabacniks[b], J.R. Matos[c], R.S. Freire[d,c], M.C.A. Fantini[b]

[a] Departamento de Ciências Exatas e da Terra, Universidade Federal de São Paulo, Rua Prof. Artur Riedel 275, 09972-270 Diadema, São Paulo, Brazil
[b] Instituto de Física, Universidade de São Paulo 66318, 05315-970 São Paulo, Brazil
[c] Instituto de Química, Universidade de São Paulo, 05508-900 São Paulo, Brazil
[d] CEPEMA/USP, Centro de Capacitação e Pesquisa em Meio Ambiente, Cubatão/SP, Brazil
[e] IPEN, Av. Prof. Lineu Prestes 2242, Cidade Universitária, 05508-900 São Paulo, Brazil

ARTICLE INFO

Article history:
Received 21 January 2010
Received in revised form 27 April 2010
Accepted 18 July 2010

Keywords:
Mesoporous materials
Iron oxide
Catalyst
Ozonation process

ABSTRACT

Iron was successfully incorporated in FDU-1 type cubic ordered mesoporous silica by a simple direct synthesis route. The (Fe/FDU-1) samples were characterized by Rutherford back-scattering spectrometry (RBS), small angle X-ray scattering (SAXS), N_2 sorption isotherm, X-ray diffraction (XRD) and X-ray absorption spectroscopy (XAS). The resulting material presented an iron content of about 5%. Prepared at the usual acid pH of −0.3, the composite was mostly formed by amorphous silica and hematite with a quantity of Fe^{2+} present in the structure. The samples prepared with adjusted pH values (2 and 3.5) were amorphous. The samples' average pore diameter was around 12.0 nm and BET specific surface area was of 680 $m^2\ g^{-1}$. Although the iron-incorporated material presented larger lattice parameter, about 25 nm compared to pure FDU-1, the Fe/FDU-1 composite still maintained its cubic ordered *fcc* mesoporous structure before and after the template removal at 540 °C. The catalytic performance of Fe/FDU-1 was investigated in the catalytic oxidation of Black Remazol B dye using a catalytic ozonation process. The results indicated that Fe/FDU-1 prepared at the usual acid pH exhibited high catalytic activity in the mineralization of this pollutant when compared to the pure FDU-1, Fe_2O_3 and Fe/FDU-1 prepared with higher pH of 2 and 3.5.

1. Introduction

The research and technological areas related to ordered mesoporous silica (OMS) have experienced a large expansion since the discovery of the M41S family in 1992 [1,2]. Many papers discussed the synthesis, characterization, modification and application of these materials in a variety of areas like physics, chemistry, biology and materials science [3–9]. These materials are synthesized with an ordered porous arrangement by employing structure-directing agents (templates). These building blocks can be formed by organic molecules, such as surfactants, that create many types of regular patterns, such as hexagonal, cubic and lamellar mesostructures, depending strongly on the template and synthesis conditions [4].

Among these templates, triblock copolymers present advantages in their use because the architecture of the amphiphilic triblock copolymer can be moderately adjusted to control interactions between inorganic and organic species. Furthermore, these templates create materials with much larger pore dimensions than those attained with ionic surfactants, and they can be easily removed by calcination or by an alternative and less structurally destructive solvent extraction procedure [4,5].

Metal or metal oxide nanoparticles confined inside mesoporous materials were already successfully and easily obtained by employing a synthesis method using a triblock copolymer providing materials with high surface area, stability to high temperature and accurately tuned pore size on a sub-nanometer scale [10–12]. The incorporation of metal oxide into OMS has been achieved by direct synthesis or grafting (post-synthesis), and particularly iron oxide has displayed good catalytic properties when employed in heterogeneous systems.

Several papers reported the incorporation of iron into bi-dimensional hexagonal OMS (SBA-15) using different strategies including direct synthesis [12–17]. In this work, the incorporation of iron in face centered cubic OMS (FDU-1) was chosen to be developed and tested as a heterogeneous catalyst for an ozonation process because, by this date, there are no reports on iron composite FDU-1. Additionally, the catalytic properties of the material in

* Corresponding author. Tel.: +55 11 71779031/50843759; fax: +55 11 0916749.
E-mail addresses: tsmartins@unifesp.br, tekamartins@gmail.com (T.S. Martins).

0254-0584/$ – see front matter © 2010 Elsevier B.V. All rights reserved.
doi:10.1016/j.matchemphys.2010.07.042

question are better than those of other previously reported OMS [18–20]. For example, FDU-1 has higher thermal and hydrothermal stability than SBA-15 [21,22].

In this present work, the synthesis of FDU-1 incorporated with iron oxide (Fe/FDU-1) was studied. For the sample in question, we analyzed the quantity and the structure and local order of the iron species present within the mesoporous silica, as well as the catalytic properties of this heterogeneous system. Thus, the main objective of this paper is to report on the synthesis, characterization and efficiency of this material as a catalyst in the complete oxidation of azo dyes by an ozonation process.

The removal of azo dyes from effluents is important due to their mutagenic and carcinogenic properties together with their intense coloration [23]. Ozone has been extensively studied in the oxidation of different pollutants, principally because ozone is a very powerful oxidizing agent ($E^0 = 2.08$ V) [24]. In an aqueous phase, ozone can be decomposed to oxygen and radical species such as the hydroxyl radical ($E^0 \cong 2.7$ V) [25]. A direct reaction is usually very selective and reaches a limited mineralization degree of refractory pollutants, especially in acidic solutions. An indirect reaction has been more effective due to faster and relatively unselective pollutant oxidation reactions. Ozone decomposition in an aqueous phase is affected by many factors including pH, initial ozone concentration, the presence of ultraviolet radiation, and the type and concentration of the material that promoted the decomposition [25–28].

Nowadays, ozonation in the presence of metals or metal oxides are promising approaches to improve the complete oxidation of pollutants by ozonation. Some studies showed that several metals in solution or in a solid phase of various forms (metallic salts, oxide solid and supported metal) can catalyze ozone reactions [25,28–30]. Heterogeneous catalysts are becoming one of the most attractive and promising alternatives because they offer several advantages compared to their homogeneous counterparts, such as ease of recovery and recycling and enhanced stability [29–31].

In this work, we propose the use of Fe/FDU-1 as a catalyst in the ozonation of an azo dye compound.

2. Experimental

2.1. Synthesis

In this work, three Fe/FDU-1 samples were prepared using two synthesis methodologies: first, the usual acid pH of −0.3 was fixed [20] and, second, the pH was adjusted to the values of 2 and 3.5.

The idea to change the pH was based on the fact that non soluble $Fe(OH)_3$ would precipitate at the same time the silica precursor hydrolyses to form the mesostructure. Therefore, iron would be incorporated inside the walls forming a robust material which would probably have better catalytic properties. Nevertheless, this change of pH did not lead to samples with improved catalytic activity, a result that could be related to the fact that iron is more active on the surface and, also, to the crystalline structure of the formed iron compound, as shown below.

Fe/FDU-1 samples were synthesized using tetraethyl orthosilicate (TEOS, 98% Aldrich) and iron chloride ($FeCl_3.6H_2O$, Aldrich, ~5% in molar of Fe^{3+}) as silica and iron precursors respectively. Nonionic triblock copolymer surfactant $EO_{39}BO_{47}EO_{39}$ (B50-6600, Dow Chemical Co.) was used as the structure-directing agent. Concentrated HCl aqueous solution (Vetec, 2 mol L^{-1}) was used as the acid source. All reagents were utilized as received.

The synthesis procedure of the Fe/FDU-1 sample prepared at a fixed pH of −0.3 was: 2 g of B50-6600 was dissolved in 120 g of HCl 2 mol L^{-1} and stirred at room temperature until a homogeneous mixture was obtained. Subsequently, iron chloride was added, and the system was stirred for 30 min followed by the addition of TEOS (8.9 mL). The stirring continued for about 24 h. The resulting mixture was transferred to a Teflon-lined autoclave and heated at 100 °C for 6 h without stirring. After hydrothermal treatment, the resultant solid was separated from the solution by solvent evaporation at 80 °C in a water bath. The solid was calcined at 540 °C for about 4 h under nitrogen, and then atmosphere was switched to air, maintaining the furnace temperature for two more hours.

The other two Fe/FDU-1 samples were prepared at pH values of 2 and 3.5, following the procedure described before, but adding a base (NH_4OH) solution after the TEOS addition until the pH reached the pre-determined values.

2.2. Characterization

In order to determine the material's composition, Rutherford back-scattering spectrometry (RBS) measurements were performed using a He^+ beam with an energy $E = 2.2$ MeV, charge $Q = 20$ μC, current $I = 30$ nA and detection angle of 170°. The RBS data were analyzed by the SIMRA routine [32] and the atomic densities (atoms cm^{-2}) of Si, O, Cl and Fe were obtained.

Small angle X-ray scattering (SAXS) measurements were carried out with a rotating anode X-ray generator, operating at 10 kW. The wavelength of the copper K_α radiation was $\lambda = 0.15418$ nm. An image plate detector was used to record the scattered intensity as a function of the scattering vector $q = (4\pi \sin\theta)/\lambda$, θ being half the scattering angle, and the measurement period lasted for 2 h. Line focus geometry was used and the system was collimated by slits. A vacuum path between the sample and the detector was utilized. The sample to the detector distance (~501 mm) was chosen in order to record the scattered intensity for q values ranging from 0.08 to 3.5 nm^{-1}. The samples were placed inside a quartz tube, 2 mm in diameter. The scattering of the sample holders was subtracted from the total measured intensities. All data were corrected for absorption effects.

Nitrogen sorption isotherms were measured at 77 K, using nitrogen of 99.998% purity, on a Micromeritics ASAP 2010 volumetric sorption analyzer. Measurement was performed in the range of relative pressure from 10^{-6} to 0.99. Before the sorption measurement, the sample was outgassed at 200 °C in the port of the sorption analyzer. Specific surface area was evaluated using the BET method [33]. The total pore volume, V_{Pt} ($cm^3\ g^{-1}$), was estimated from the amount adsorbed at the relative pressure of 0.99 and the microporous volume, V_{mi} ($cm^3\ g^{-1}$), was calculated using the standard reduced adsorption data. Pore size distribution (PSD) was calculated using the BJH algorithm [34] with the relation between capillary condensation pressure and pore diameter established by Kruk et al. [35,19].

Powder X-ray diffraction (XRD) patterns were obtained on a Rigaku diffractometer, in a Bragg–Brentano geometry, with CuK_α ($\lambda = 0.15418$ nm) radiation, at 40 kV and 30 mA, for 2θ between 5° and 95° with step scanning mode of 0.05° and time intervals of 10 s.

X-ray absorption near edge (XANES) and extended X-ray absorption fine structure (EXAFS) spectra were measured at the D04B-XAFS1 beamline [36] (Brazilian Synchrotron Light Laboratory, LNLS, Campinas – SP, Brazil) in transmission mode using Si (1 1 1) monochromator. The nominal photon flux of the beamline is 3×10^9 photons/(s.mrad.100 mA) at 6 keV. The energy range was 7000 to 8200 eV for Fe K edge and the energy was calibrated with an iron foil. Data were collected for Fe/FDU-1 and α-Fe_2O_3 samples. The measurements were carried out at room temperature using energy steps from 0.3 to 4 eV, depending on the energy range (XANES and EXAFS) and $E/\Delta E = 5000$–10000. The integration time varied from 1 to 3 s at different energy ranges. Three spectra were measured for each sample and the average spectrum was used to perform the data analysis. EXAFS data analysis were performed using the WINXAS code [37] and FEFF8 software [38]. Both pre- and post-edge were subtracted from raw data. For the pre-edge region, a linear fit of the absorption signal was subtracted from the experimental data and, a fifth-order polynomial was used for the post-edge removal. The first and second shells around Fe were analyzed for both samples and reference. The selected Fourier transform (FT) windows for Fe K edge analysis was 2.4–12.4 $Å^{-1}$ and 1.0–3.85 Å in k- and R-space, respectively. A k^3-weighted oscillation was used to calculate the Fourier transform. The coordination numbers were fixed equal to those of Fe_2O_3 crystalline reference and bond length (R), Debye–Waller factor (σ) and inner potential shift (E_o) were used as free parameters in the fitting procedure. This last parameter was regarded as equal for the same type of atoms having close distances at the same broad coordination sphere.

2.3. Catalysis test

Black Remazol B (DyStar Company) was chosen as a model dye to perform the catalysis tests. Its structure is shown in Fig. 1.

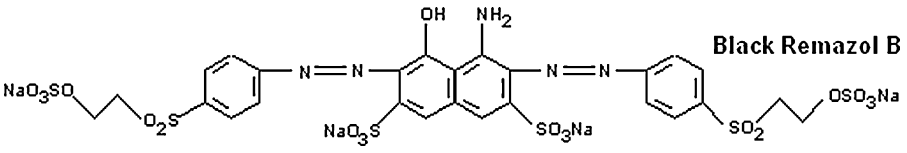

Fig. 1. Structure of the dye Black Remazol B compound.

Table 1
Interplanar spacing (d_{hkl}), lattice parameter (a_{hkl}) and mass percent of elements determined for Fe/FDU-1.

Sample	SAXS				RBS			
	(hkl)	(1 1 1)	(2 2 0)	(3 1 1)	%[Si]	%[O]	%[Cl]	%[Fe]
Fe/FDU-1	$d_{(hkl)}$ (nm)	14.5	8.0	7.0	42.2	52.5	0.6	4.6
	$a_{(hkl)}$ (nm)	25.2	22.8	23.1				

Ozone was generated from pure oxygen using a MV06 equipment (Multivacuo, Sao Paulo, Brazil) based in the corona electric discharge method. This apparatus has the capacity of generating ozone in the range between 0.10 and 2.20 g h^{-1}. The ozone produced was determined spectrophotometrically at 258 nm (ε = 3000 L mol^{-1} cm^{-1}) in its gaseous phase by passing the mixture of oxygen and ozone through a flow cell [39]. The oxygen flow rate was adjusted to 50 (±3) L h^{-1} which resulted in an ozone concentration of 20 mg L^{-1}.

The ozonation treatment was carried out using a tubular reactor of 500 mL equipped with a sintered glass disperser that releases the gas from the bottom to the top of the reactor. All experiments were performed at 25 °C and using 350 mL of 100 mg L^{-1} Black Remazol aqueous solution with pH adjusted to 3 (by HCl 12 mol L^{-1} addition). In the catalytic tests, 35 mg of Fe/FDU-1 was used, which corresponds to 100 mg L^{-1} in the reactor. The samples were collected at different times and the degree of mineralization was evaluated measuring the concentration of total organic carbon (TOC) following the standard 5310B method from Standard Methods for the Examination of Water and Wastewater [40].

3. Results and discussion

The three samples prepared were characterized by SAXS, XRD, RBS and nitrogen sorption isotherms, and evaluated as catalysts in the ozonation of an azo dye compound.

Comparing the structural parameters of the three Fe/FDU-1 samples, only small differences (less than 5%) in the interplanar spacing (d_{hkl}) and lattice parameters (a_{hkl}) values were observed. All the samples presented similar values of surface areas and amount of iron inside the silica matrix. The sample prepared in a higher acidic condition only presented a small increase (~5%) of surface area.

For the samples prepared with pH variation, the X-ray diffractograms showed only the broad band centered around 23°, which corresponds to the amorphous SiO_2 walls, typical of the FDU-1 material. However, the sample prepared at fixed acid pH, the diffractogram displayed the peaks typical to crystalline Fe_2O_3 (hematite).

The catalytic performances of the samples prepared at pH 2 and 3.5 were identical.

On the other hand, the sample prepared at fixed pH of −0.3 presented an improvement on catalytic activity of about 25%, showing that iron was incorporated into SiO_2 matrix in a different and more efficient form compared to the former two samples. The hypothesis to explain this better result is based on the fact that this sample is formed by polycrystalline instead of amorphous, hematite, in addition to the presence of iron compounds at the pore' surfaces. Even though the three samples were fully characterized, the following sections will only display the complete results and focus the discussion on the sample that presented the best catalytic properties.

3.1. Iron content and structural properties

RBS results are listed in Table 1. The amounts of O and Si are in agreement with the expected stoichiometry of the main compound, that being SiO_2. The low Cl content observed is associated with the synthesis process since the sample was not washed and the iron precursor and hydrochloric acid (HCl) contain Cl.

SAXS data of calcined Fe/FDU-1 are presented in Fig. 2 after background subtraction, and the structural parameters are summarized in Table 1. The diffraction peaks were indexed to (1 1 1), (2 2 0) and (3 1 1) reflections based on a face centered cubic (*fcc*) structure, space group *Fm3m*. The atomic distances were compared to those

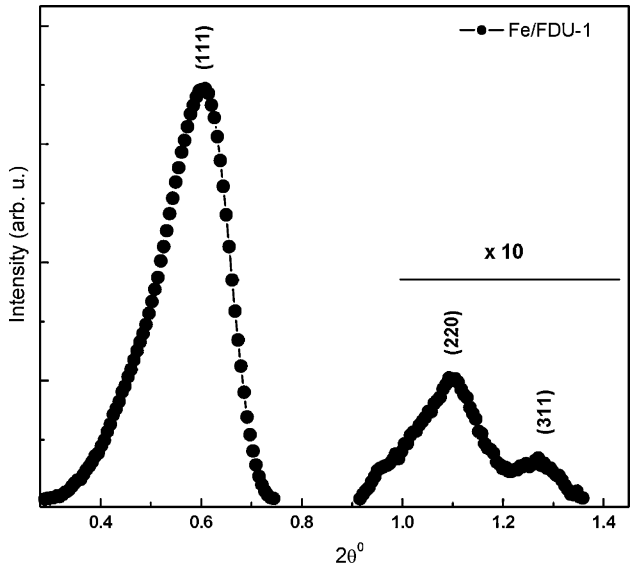

Fig. 2. SAXS of calcined Fe/FDU-1.

of FDU-1 reported by Matos et al. [18]. The calcined Fe/FDU-1 sample presented larger lattice parameter due to larger pore sizes when compared to pure calcined FDU-1 ($a \sim 21.6$ nm) [18].

The structural properties determined from N_2 sorption data of the calcined Fe/FDU-1 sample are summarized in Table 2. The primary mesopore volume, V_p (cm^3 g^{-1}), was estimated from the difference between V_{Pt} (total volume pore) and V_{mi} (micropore volume). The primary mesopore diameter (w_d), the average pore wall thickness (b) and minimal wall thickness (b_{min}) in the *fcc* structure were calculated using the equations described in reference [19]. N_2 sorption isotherm of this material is shown in Fig. 3. Such isotherm is typical of materials having large, uniform, cage-like mesopores with cubic structure, and this isotherm was similar to the pure FDU-1 reported by Matos et al. [18]. As expected, the micropore volume

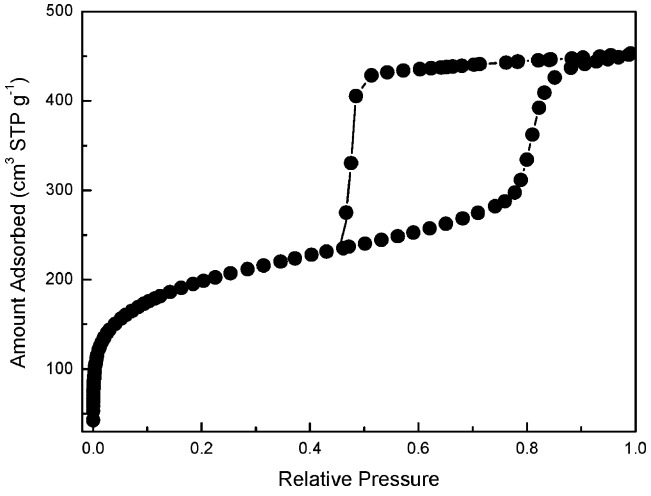

Fig. 3. N_2 sorption isotherm at 77 K for calcined Fe/FDU-1.

Table 2
Structural properties determined from N_2 sorption isotherm data for calcined Fe/FDU-1[a].

Sample	$S_{(BET)}$ ($m^2\ g^{-1}$)	W_d (nm)	V_{mi} ($cm^3\ g^{-1}$)	V_{Pt} ($cm^3\ g^{-1}$)	V_p ($cm^3\ g^{-1}$)	b (nm)	b_{min} (nm)
Fe/FDU-1	677	11.8	0.095	0.701	0.606	4.8	1.9

[a] S_{BET}, BET specific surface area; W_d, pore width; V_{mi}, micropore volume; V_{Pt}, total volume pore; V_p, primary mesopore volume; b, pore wall thickness; b_{min}, minimal wall thickness.

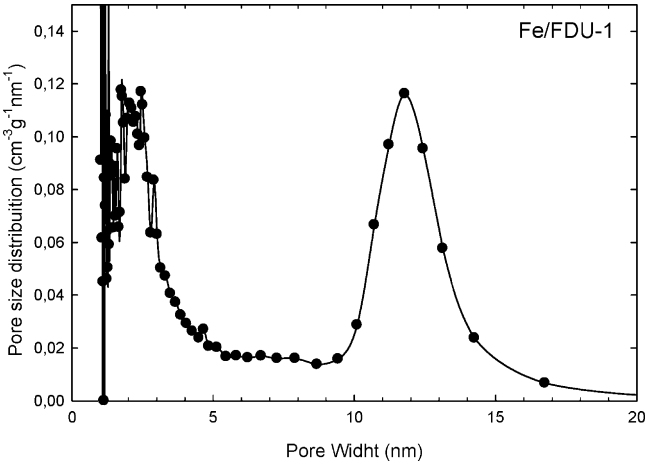

Fig. 4. Pore size distribution calculated from N_2 sorption isotherm of calcined Fe/FDU-1 sample.

is higher in the Fe/FDU-1 sample [18]. All other parameters are quite similar. The pore size distribution is shown in Fig. 4.

XRD patterns of both FDU-1 and Fe/FDU-1 samples are shown in Fig. 5. The large band present in the smaller angles is due to the amorphous silica. The Fe/FDU-1 diffractogram displays peaks of poly-crystalline Fe_2O_3 (hematite), besides non-identified amorphous (a, labeled in Fig. 5) and other Fe (*, labeled in Fig. 5) poly-crystalline minority phases. These results show that when iron chloride is added to the polymer, during the preliminary step of the synthesis, poly-crystalline iron oxide is obtained in the mesoporous walls.

The local atomic structure of the Fe inside Fe/FDU-1 silica was investigated by X-ray absorption spectroscopy (XAS). Knowledge of the material structure is fundamental to understand the chemical processes involved in the catalytic reactions. Therefore, many works were devoted to XAS analysis of Fe incorporation

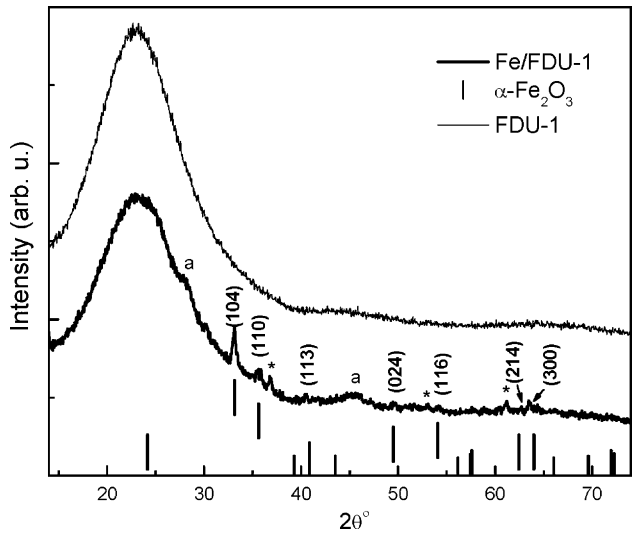

Fig. 5. X-ray diffraction results of calcined Fe/FDU-1.

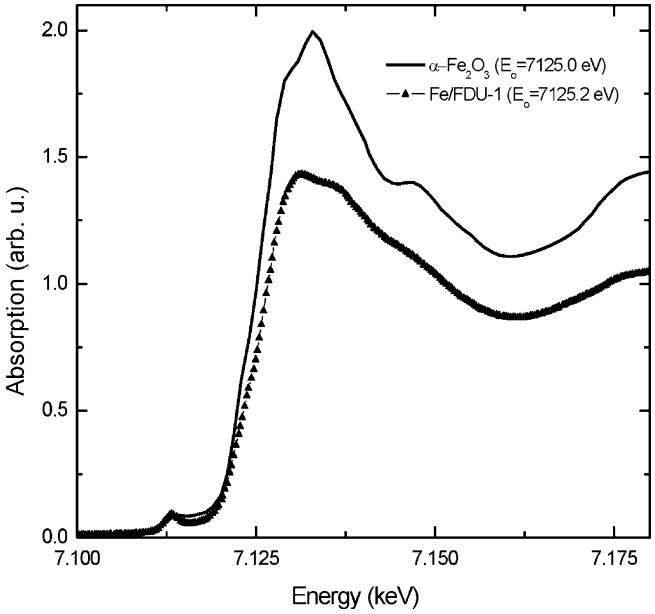

Fig. 6. XANES data at Fe K edge.

in porous systems [15,17,41–50] and its application in catalytic processes. Ordered cubic mesoporous Fe_2O_3 with crystalline walls were already obtained [15,48], but the catalytic properties of amorphous and crystalline phases were not compared.

Fig. 6 shows the XANES data. The determined energy edge (E_0 = 7125 eV) of the Fe/FDU-1 sample is identical, within the experimental uncertainty, to the reference Fe_2O_3 (α phase) and similar to other reported data [41,45]. The pre-edge peak at 7113 eV reveals that the sample also contains Fe^{2+} [42,44,46].

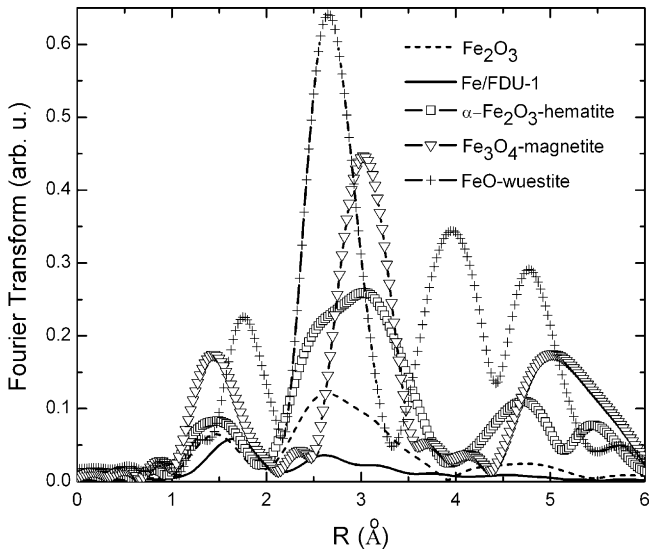

Fig. 7. Fourier transform of the EXAFS signal from experimental data and calculated standards.

Table 3
Structure parameters of reference iron compounds. First Fe coordination shell where $N_{O(i)}$ is the oxygen coordination number and $R_{O(i)}$ the distance Fe–$O_{(i)}$.

Reference	Crystal structure	$N_{O(1)}$	$R_{O(1)}$ (Å)	$N_{O(2)}$	$R_{O(2)}$ (Å)
α-Fe_2O_3 hematite	Hexagonal (R-3c)	3	1.9443	3	2.1126
Fe_3O_4 magnetite	Cubic (Fd3m)	4[a]	1.8982	6[b]	2.0544
FeO wuestite	Cubic (Fm3m)	6	2.1660	–	–

[a] Fe^{2+}.
[b] Fe^{3+}.

Fig. 7 depicts the Fourier transform (TF) of the measured sample in comparison with the calculated TF of some reference iron compounds: hematite, magnetite and wuestite. The relevant crystallographic data of these compounds are given in Table 3. It's clear from Fig. 7 that the analyzed sample has a local atomic structure more similar to α-Fe_2O_3. But the presence of Fe^{2+}, already detected by XANES, shifts the first shell distances towards higher values, as in FeO. In addition, the fitting of the first and second coordination spheres (Fe_2O_3 and Fe/FDU-1) was performed with the FEFF8 software. In this calculation the reference single paths were determined using the α-Fe_2O_3, up 4 Å. Some diffusion paths were removed from the fitting since they did not contribute to improve the simulation quality.

The fitting results are shown in Fig. 8 and the parameters in Table 4. The results demonstrate that the distances of neighbors closer to iron, FeO, tend to have values more similar to Fe_3O_4 (see Table 4), in agreement with the presence of Fe^{2+} and Fe^{3+}. The closer oxygen atoms exhibit larger disorder compared to the outer ones at larger distances from iron. Moreover, the static disorder around Fe is higher than that observed for the Fe_2O_3 standard, which can be attributed to smaller crystallite sizes compared to the reference.

3.2. Catalytic performance

An amount of 100 mg L^{-1} of Fe/FDU-1, pure FDU-1 and Fe_2O_3 were separately tested for catalytic performance during the ozona-

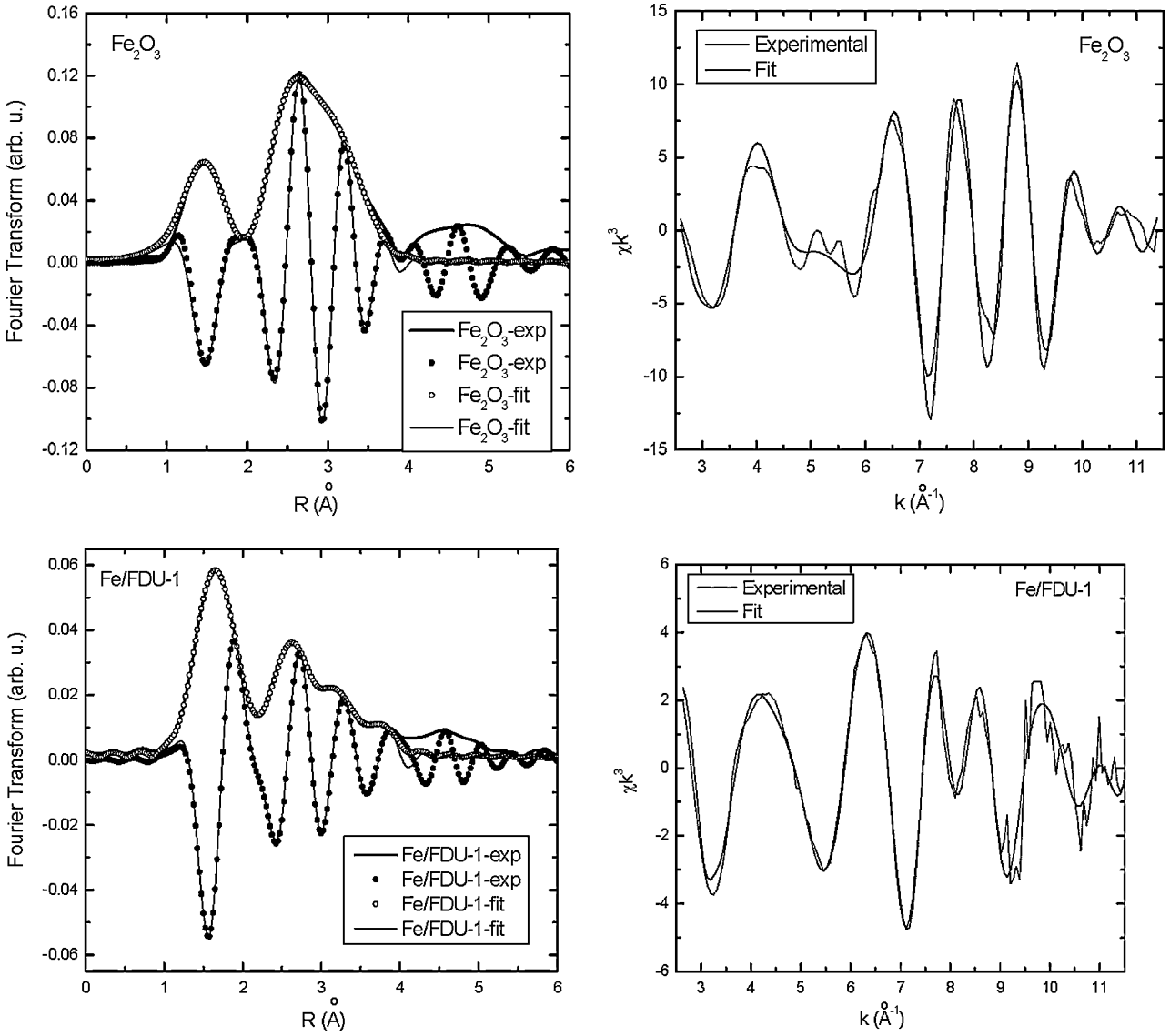

Fig. 8. Comparison between experimental and theoretical amplitude, real part and EXAFS function, calculated with FEFF8 code.

Table 4
Simulation results of EXAFS data, with fixed coordination numbers (N) and constraints on energy shift (E_o).

Theoretical α-Fe_2O_3					Fe_2O_{3exp}		Fe/FDU-1		
Path	Bond	AR[a]	N	R (Å)	σ (Å)	E_o (eV)	R (Å)	σ (Å)	E_o (eV)
1	Fe–O	100	3	1.9443	0.077	4.6	1.829	0.22	9.4
2	Fe–O	83	3	2.1126	0.096	4.6	2.042	0.082	9.4
3	Fe–Fe	15	1	2.8899	0.059	1.5	2.799	0.13	−4.4
4	Fe–Fe	41	3	2.9705	0.073	1.5	2.974	0.12	−4.4
5	Fe–Fe	31	3	2.3611	0.075	1.5	3.34	0.097	−4.4
6	Fe–O	27	3	3.3977	–	–	3.421	0.11	−11.2
14	Fe–O	24	3	3.5864	–	–	3.564	0.098	−11.2
16	Fe–Fe	49	6	3.7001	0.097	1.5	3.583	0.16	−4.4
17	Fe–O	21	3	3.7836	–	–	–	–	–
22	Fe–Fe	7	1	3.9712	0.055	1.5	4.060	0.035	−4.4
28	Fe–O	17	3	4.1229	–	–	4.128	0	−11.2
33	Fe–O	14	3	4.3942	–	–	–	–	–

[a] AR = amplitude ratio.

tion of the Black Remazol aqueous solution at pH 3. The dye decolorization degree was evaluated (data not shown) independently to the experimental set. After 5 min a fast and total dye solution discoloration was observed. It's well known that direct reaction of molecular ozone is very effective in the oxidation of rich-electrons centers (such as the azo dye chromophore group). Usually molecular ozone reacts with many color-causing groups changing the molecular structure, leading to colorless degraded products which still remain in the solution without significant change in the organic carbon content. Nevertheless, mineralization is generally much lower than color removal. The results of TOC are presented in Fig. 9, which demonstrates that after 5 min of treatment time, the mineralization degree is very similar to the different ozonation experimental approaches, with a maximum TOC removal of 16% when the Fe/FDU-1 material was employed. The advantage of using this material was clearly observed for longer treatment times. The TOC removal by the Fe/FDU-1 was much faster and effective than that obtained by single ozonation or ozonation in presence of Fe_2O_3 and FDU-1. For ozonation treatment using pure mesoporous silica or Fe_2O_3 in solution, the mineralization of the dye was about 40% after 1 h of treatment, a level very similar to that obtained by the direct ozonation (performed at pH 3). On the other hand, for the same treatment time the ozonation in the presence of modified silica with Fe presented mineralization of 70%. Control adsorption experiments were carried out and no significant TOC content variation was observed after 2 h without ozone presence.

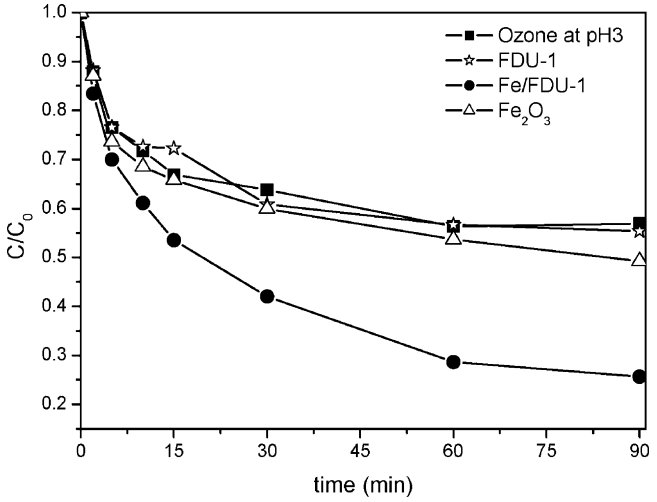

Fig. 9. Variation of total organic carbon as function of the treatment time. Ozonation processes using 100 mg L^{-1} Black Remazol B aqueous solution pH 3 in the presence of ozone only, pure silica, Fe/FDU-1 and Fe_2O_3.

These results show that the iron oxide incorporated in mesoporous silica works as a better catalyst than pure iron oxide for the catalytic ozonation of the Black Remazol azo dye compound. An explanation for the improvement of the catalytic properties of the Fe/FDU-1 material is related to the high surface area of the silica support. The mesoporous silica support is able to disperse the iron active phase in order to increase its contact with the Black Remazol azo dye compound. Also, as reported in the literature, the interaction between the silica support and the active iron improves the catalytic performance [50]. For example, the enhancement of removal efficiency of this compound in the presence of Fe/FDU-1 can be due to the increase of ozone decomposition into highly oxidant radical species (such as •OH) in the reaction medium.

4. Conclusion

The incorporation of iron in FDU-1 was successfully achieved by a direct synthesis procedure building a well defined crystalline mesoporous structure. The Fe/FDU-1 walls are formed mostly by amorphous silica, poly-crystalline hematite and other less crystalline phases. The catalytic performance for the mineralization of an azo dye employing this new Fe/FDU-1 material is higher than pure FDU-1 and Fe_2O_3, showing the promising use of this composite for environmental decomposition of azo compounds.

The methodology of synthesis presented here constitutes a general synthetic route that could be applied to the preparation of other catalytic systems with different metals.

Acknowledgments

The authors acknowledge the Fundação de Amparo à Pesquisa do Estado de São Paulo (FAPESP) and the Conselho Nacional de Desenvolvimento Científico e Tecnológico (CNPq) for the financial support. The Laboratório Nacional de Luz Síncrotron (LNLS), Brazil, is acknowledged for the use of D04B-XAFS1 beamline (project number 5261/06), with assistance of Dr. Gustavo de Medeiros Azevedo and Dr. Ana Paula Rodrigues.

References

[1] J.S. Beck, J.C. Vartuli, W.J. Roth, M.E. Leonowicz, C.T. Kresge, K.D. Schmitt, C.T.-W. Chu, D.H. Olson, E.W. Sheppard, S.B. McCullen, J.B. Higgins, J.L. Schlenker, J. Am. Chem. Soc. 114 (1992) 10834.
[2] C.T. Kresge, M.E. Leonowicz, W.J. Roth, J.C. Vartuli, J.S. Beck, Nature 359 (1992) 710.
[3] U. Ciesla, F. Schüth, Micropor. Mesopor. Mater. 27 (1999) 131.
[4] J.K. Edler, S.J. Roser, Int. Rev. Phys. Chem. 20 (2001) 387.
[5] R.M. Grudzien, B.E. Grabicka, M. Jaroniec, J. Mater. Chem. 16 (2006) 819.
[6] L.P. Mercuri, L.V. Carvalho, F.A. Lima, C. Quayle, M.C.A. Fantini, G.S. Tanaka, W.H. Cabrera, M.F.D. Furtado, D.V. Tambourgi, J.R. Matos, M. Jaroniec, O.A. Santanna, Small 2 (2006) 254.

[7] V. Meynen, P. Cool, E.F. Vansant, Micropor. Mesopor. Mater. 125 (2009) 170.
[8] L.C. Cides da Silva, T.S. Martins, M. Santos Filho, E.E.S. Teotônio, P.C. Isolani, H.F. Brito, M.H. Tabacniks, M.C.A. Fantini, J.R. Matos, Micropor. Mesopor. Mater. 92 (2006) 94.
[9] A.Z. Abdullah, H. Abdullah, S. Bhatia, Mater. Chem. Phys. 103 (2007) 375.
[10] T. Tsoncheva, L. Ivanova, J. Rosenholm, M. Linden, Appl. Catal. B 89 (2009) 365.
[11] F. Jiao, H. Frei, Angew. Chem. Int. 48 (2009) 1841.
[12] J. Li, X. Wei, Y.S. Lin, D. Su, J. Membr. Sci. 312 (2008) 186.
[13] H. Lim, J. Lee, S. Jin, J. Kim, J. Yoon, T. Hyeon, Chem. Commun. 4 (2006) 463.
[14] L. Chmielarz, P. Kustrowski, R. Dziembaj, P. Cool, E.F. Vansant, Appl. Catal. B 62 (2006) 369.
[15] F. Jiao, A. Harrison, J.C. Jumas, A.V. Chadwick, W. Kockelmann, P.G. Bruce, J. Am. Chem. Soc. 128 (2006) 5468.
[16] Y. Wang, W. Yang, L. Yang, X. Wang, Q. Zhang, Catal. Today 117 (2006) 156.
[17] T. Tsoncheva, J. Rosenholm, C.V. Teixeira, M. Dimitrov, M. Linden, C. Minchev, Micropor. Mesopor. Mater. 89 (2006) 209.
[18] J.R. Matos, M. Kruk, L.P. Mercuri, M. Jaroniec, L. Zhao, T. Kamiyama, O. Teresaki, T.J. Pinnavaia, Y. Liu, J. Am. Chem. Soc. 125 (3) (2003) 821.
[19] M. Kruk, E.B. Celer, M. Jaroniec, Chem. Mater. 16 (2004) 698.
[20] M.C.A. Fantini, J.R. Matos, L.C. Cides da Silva, L.P. Mercuri, G.O. Chiereci, E.B. Celer, M. Jaroniec, Mater. Sci. Eng. B 112 (2004) 106.
[21] C. Yu, Y. Yu, D. Zhao, Chem. Commun. 7 (2000) 575.
[22] C. Yu, Y. Yu, L. Miao, D. Zhao, Micropor. Mesopor. Mater. 44 (2001) 65.
[23] R.S. Freire, W.S. Pereira, J. Braz. Chem. Soc. 17 (2006) 832.
[24] S.G. Moraes, R.S. Freire, N. Durán, Chemosphere 40 (2000) 369.
[25] A. Mahmoud, R.S. Freire, Quim. Nova 30 (2007) 198.
[26] R.S. Freire, A. Kunz, N. Durán, Environ. Technol. 21 (2000) 717.
[27] R.S. Freire, L.T. Kubota, N. Dúran, Environ. Technol. 22 (2001) 897.
[28] C.-H. Wu, C.-Y. Kuo, C.-L. Chang, J. Hazard. Mater. 154 (2008) 748.
[29] M.H. Khan, J.Y. Jung, Chemosphere 72 (2008) 690.
[30] J. Qu, H. Li, H. Liu, H. He, Catal. Today 90 (2004) 291.
[31] F.J. Beltrán, F.J. Rivas, R. Montero-de-Espinosa, Ind. Eng. Chem. Res. 42 (2003) 3218.
[32] M. Mayer, SIMNRA, a simulation program for the analysis of NRA, RBS and ERDA, in: J.L. Duggan, I.L. Morgan (Eds.), Proceedings of the 15th International Conference on the Application of Accelerators in Researchand Industry, American Institute of Physics Conference Proceedings, vol. 475, New York, 1991, p. 541.
[33] S. Brunauer, P.H. Emmet, E. Teller, J. Am. Chem. Soc. 60 (1938) 309.
[34] E.P. Barret, L.G. Joyner, P.H. Halenda, J. Am. Chem. Soc. 73 (1951) 309.
[35] M. Kruk, M. Jaroniec, A. Sayari, Langmuir 13 (1997) 6267.
[36] H.C.N. Tolentino, J.C. Cezar, V. Compagnon-Cailhol, E. Tamura, M.C.M. Alves, J. Synchrotron Radiat. 5 (1998) 521.
[37] T. Ressler, J. Synchrotron Radiat. 5 (1998) 118.
[38] A.L. Ankudinov, B. Ravel, J.J. Rehr, S.D. Conradson, Phys. Rev. B: Condens. Matter Mater. Phys. B 58 (1998) 7665.
[39] A. Kunz, P. Peralta-Zamora, S.G. de Moraes, N. Duran, Quim. Nova 25 (2002) 78.
[40] Standard Methods for the Examination of Water and Wastewater, 2002.
[41] S.T. Wong, J.F. Lee, S. Cheng, S.Y. Mou, Appl. Catal. A 198 (2000) 115.
[42] G. Wirnsberger, K. Gaterrer, H.P. Fritzer, W. Grooger, B. Pillep, P. Behrens, M.F. Hansen, C.B. Koch, Chem. Mater. 13 (2001) 1453.
[43] Y. Wang, Q. Zhang, T. Shishido, K. Takehira, J. Catal. 209 (2002) 186.
[44] G. Berlier, G. Spoto, S. Bordiga, G. Riccchiardi, P. Fisicaro, A. Zecchina, I. Rossetti, E. Selli, L. Forni, E. Giamello, C. Lamberti, J. Catal. 208 (2002) 64.
[45] G. Berlier, G. Spoto, P. Fisicaro, S. Bordiga, A. Zecchina, E. Giamello, C. Lamberti, Microchem. J. 71 (2002) 101.
[46] Q. Zhang, W. Yang, X. Wang, Y. Wang, T. Shishido, K. Takehira, Micropor. Mesopor. Mater. 77 (2005) 223.
[47] G. Berlier, M. Pourny, S. Bordiga, G. Spoto, A. Zecchina, C. Lamberti, J. Catal. 229 (2005) 45.
[48] F. Jiao, J.C. Jumas, M. Womes, A.V. Chadwick, A. Harrison, P.G. Bruce, J. Am. Chem. Soc. 128 (2006) 12905.
[49] Y. Izumi, D. Masih, K. Aika, Y. Seida, Micropor. Mesopor. Mater. 94 (2006) 243.
[50] R. Zāvoianua, C.R. Dias, M.F. Portela, React. Kinet. Catal. Lett. 72 (2001) 201.